Water decontamination in terms of Hg (II) over thiol immobilized magnesium ferrite – Gum Arabic biosorbent: Response surface optimization, kinetic, isotherm and comparing study

Mostafa Nowroozi
Tehran University: University of Tehran
Hassan Alijani (h.alijani@scu.ac.ir)
Shahid Chamran University of Ahvaz https://orcid.org/0000-0001-5959-2862
Mostafa Hossein Beyki
Tehran University: University of Tehran
Hassan yadaei
Tehran University: University of Tehran
Farzaneh Shemirani
Tehran University: University of Tehran

Research Article

Keywords: Biosorption, Gum Arabic, L – Cysteine, Response surface methodology, Mercury

Posted Date: April 11th, 2022

DOI: https://doi.org/10.21203/rs.3.rs-1512864/v1

Water decontamination in terms of Hg (II) over thiol immobilized magnesium ferrite – Gum Arabic biosorbent: Response surface optimization, kinetic, isotherm and comparing study

Mostafa Nowroozi[a], Hassan Alijani[b*], Mostafa Hossein Beyki[a], Hassan yadaei[a], Farzaneh Shemirani[a]

[a] *School of Chemistry, University College of Science, University of Tehran, Tehran, Iran.*

[b] *Department of Chemistry, Faculty of Science, Shahid Chamran University of Ahvaz, Ahvaz, Iran*

email: h.alijani@scu.ac.ir

Abstract

Mercury thrown even at a low concentrations in water resources causes a severe threat to ecosystem hence the presented work describes a low cost and environmentally friendly clean up platform for decontamination of water in terms of mercury ions. For this purpose $MgFe_2O_4$ – Gum Arabic composite was prepared with a simple ultrasound assisted precipitation route and further modified with L-cysteine as a thiol resource to improve its adsorption characteristic. The structure of biosorbent was characterized with XRD, FESEM, VSM, EDX, and BET techniques. Effective parameters on mercury adsorption were optimized with response surface methodology (RSM) using Box-Behnken design (BBD). Maximum removal efficiency was obtained at pH of 5, contact time of 15 min and adsorbent dosage of 19 mg by magnetic GA. After thiol functionalization optimum variables changed to pH of 2, time of 15 min and dosage of 5 mg. Isotherm study indicated that mercury biosorption onto the magnetic Gum Arabic and thiol immobilized sorbent followed Langmuir and Freundlich model with adsorption capacity of 96 and 250 mg g^{-1}, respectively. Results for kinetic study revealed that mercury adsorption followed pseudo – second order model. To study the ability of biosorbent as a reusable compound a mixture of HCl (0.5 mol L^{-1}) and thiourea (2%) was employed to release the adsorbed ions from the sorbent surface moreover, it showed 90% removal efficiency after three cycles of sorption and desorption which confirmed the presented composite is a reusable biosorbent.

Keywords: Biosorption, Gum Arabic, L – Cysteine, Response surface methodology, Mercury.

1. Introduction

Contamination of surface and ground water with heavy metals is a special concern in terms of environmental protection. Among heavy metals mercury is a priority toxic compound as the European Union (EU) legislation appointed the allowable level of 0.07l μg/L in surface water [1,2]. Mercury is a high reactive and volatile metal that is relatively soluble in living tissues and water resources hence it can causes damage to kidney and nervous system as well as birth and chromosome defects [3, 4]. Mercury thrown in environment has been increased dramatically in recent decades owe to extensive development in textile, fertilizer, leather and military industry [5–7]. Hazardous effects of mercury as well as its high tendency for accumulation onto living ecosystems and food chains persuaded researchers to find effective methods for remediation of mercury contaminants [8, 9]. Up to now several technologies such as coagulation, precipitation, ion exchange, and adsorption have been developed for mercury removal [10]. In view of the economical aspects and environmental benign; adsorption is more suitable process for water treatment comparing with the mentioned techniques [11, 12]. Numerous adsorbents such as carbon based materials, silica gel, chelating resins, and fibers, have been applied in mercury adsorption process [13–18]. In spite of worthiness of the most mentioned adsorbents in literature some of them show weaknesses like low capacity and high equilibrium time causes low desire to choose them for water treatment hence it is quite necessary to develop novel adsorption based plane for water treatment [19]. In recent decades a growing attention was paid to the use of nanostructures for clean water supply. This is because of the unique properties of nanosorbents such as high surface area and great active sites which made the adsorption process fast, simple and more efficient [20–23].

Biosorption, an adsorption process that uses materials with natural resources, attracted a great attention for water decontamination since it uses inexpensive and environmentally friendly material. The most employed biosorbents for metal adsorption including, rice husk, chitosan, wool, cellulose, Jujuba seeds, Gum Arabic (GA) and so on [24–26]. The GA is a natural negatively charged polysaccharide which has been utilized widely in food ingredient and pharmaceutical industries owe to its biocompatibility [27]. However, relative water solubility limits its technological applications as led to unsatisfactory adsorption behavior [28]. The mentioned weakness can be eliminated by preparing organic/inorganic composite of GA. In fact the prepared composite combine outstanding traits of two components through increases of surface area and active sites [29]. Magnetic composite is an appropriate choice to improve the adsorption properties

of GA since it exhibited easy separation and large flexibility in further surface modification. One of the suitable candidates in magnetic GA preparation is $MgFe_2O_4$ as a subset of spinel-ceramic ferrites with high corrosive stability, biocompatibility and eco-friendly due to the presence of Mg^{2+} instead of heavy metals [30]. The above-described viewpoints convinced our research group to prepare magnetic $MgFe_2O_4$ – GA composite for mercury removal. In order to improve the mercury adsorption property of the magnetic GA, it was reacted with L- cysteine (LC) as a low toxic thiol carrier. In fact sulfur functional group of LC react with the mercury ions through soft acid–soft base interactions [31] [32]. In other words, combination of LC with magnetic GA generates an interesting advance material with improved adsorption properties relative to the unmodified magnetic GA. Effective parameters on mercury adsorption was optimized with response surface methodology (RSM) using Box–Behnken Design (BBD). Moreover, the kinetic and isotherm models were studied and results were compared with each other.

2. Experimental

2.1. Materials and instruments

Distilled water was used to prepare all stock solutions and required aqueous media for synthetic process. GA was supplied from a local market in Tehran, Iran. Ferric nitrate ($Fe(NO_3)_3.9H_2O$), magnesium nitrate ($Mg(NO_3)_2$), epichlorohydrin (ECH), sodium hydroxide (NaOH) and L- Cysteine were supplied from Merck (Darmstadt, Germany) and used to prepare magnetic modified GA. To prepare stock solution of Hg^{2+} with concentration of 1000 mg/L; mercury chloride (Merck) was dissolved in distilled water at pH of 3 using hydrochloric acid (HCl). Ethanol was supplied from Bidestan Company (Qazvin, Iran).

The morphology of the prepared magnetic modified GA was characterized at the accelerating voltage of 15 KV with Field Emission Scanning Electron Microscopy (FE-SEM) using Mira 3 Tescan; Czech Republic. N_2 adsorption/desorption experiment was performed with the Brunauer, Emmett and Teller (BET) method. The magnetic behavior of the composite were studied by Vibrating Sample Magnetometer (VSM, model MDKFD, Iran). Crystallinity of the composite was studied with Cu-Ka (λ=1.540589 Å) radiation in the 2θ range of 2-100˚ using a powder X-ray diffraction analyzer (Phillips powder diffractometer, X' Pert MPD). Elemental component of the prepared composite was determined with Energy dispersive X-ray spectrometry (EDX) using Oxford ED-2000 instrument (England). The pH adjustments were performed with a digital pH-

meter (model 692, metrohm, Herisau, Switzerland). Magnetic separation was assisted with external magnetic field using a neodymium-iron-boron ($Nd_2Fe_{12}B$) magnet.

2.3. Preparation of magnetic GA and modified composite

Magnetic GA was synthesized by a simple ultrasound assisted coprecipitation method. For this purpose about 2.0 g of GA was dissolved in 100 mL distilled water under magnetic stirring at 50°C. Then 0.64 g of $Mg(NO_3)_2$ and 2.0 g of $Fe(NO_3)_3.9H_2O$ was dissolved in 50 mL water have been dripped to the GA solution at room temperature. To assisted adsorption of the ions onto GA structure, the mixture was stirred for 10 min then 25 mL of NaOH solution (2 M) was added to GA – metal ions solution and the mixture was sonicated at 60ºC for 1h. The prepared magnetic GA was collected and washed with distilled water and ethanol then dried at 70°C for 3h.

Thiol immobilized magnetic GA was prepared using ECH as a linker through a refluxing route. To activation of hydroxyl functional groups on the magnetic GA surface, 2.0 g of magnetic GA was dispersed in 100 mL of NaOH solution (0.2 mol/L) using ultrasound wave within 1h. After cooling the mixture to room temperature, 5 mL of ECH was added and the mixture was stirred at room temperature for 12h. The prepared chloro magnetic GA was washed once with ethanol and redispersed in the 50 mL of ethanol – distilled water (1:1) solution containing 2.0 g of LC. The mixture was refluxed at 50°C under magnetic stirring for 24h then collected, washed with distilled water twice and ethanol once then dried at 80°C for 6h.

2.4. Adsorption experiments

Optimization of effective parameters on the adsorption efficiency was performed by RSM tests using BBD. A design expert 7.0 software was employed and three parameter including pH, contact time and adsorbent dosage were selected as effective parameters. Optimization experiments were performed at 17 designed runs, 5 center points and one block. Sample solutions were 10 mL with the mercury concentration of 20 mg/ L. The values of the parameters are shown in Table 1.

Table 1: variables of Box-Behnken Design

	Parameter	-Level	+Level
A	pH	2	8
B	Time	5	20
C	Dose	5	20

Isotherm and kinetic data was extracted at the optimum value of parameters. Mercury concentration was 1 - 150 mg/ L with volume of 10 mL. After equilibrium the concentration of the mercury ions in the supernatant is determined by ICP–AES analysis. The removal percentage (%R) is calculated based on the initial (C_0) and remained concentration of mercury after equilibrium (C_e) using the following equation.

$$\%R = \frac{C_0 - C_e}{C_0} \times 100 \quad (1)$$

3. Results and discussion

3.1. Characterization

Elemental analysis of the magnetic GA and final composite was performed with the EDX analysis. According to results at Fig.1, magnetic GA composed of C, O, Fe and Mg which is corresponded to the component of the employed raw material. After preparing LC immobilized magnetic GA two new peaks corresponded to the elements of S and N is appeared which proves that the nanocomposite preparation was successful.

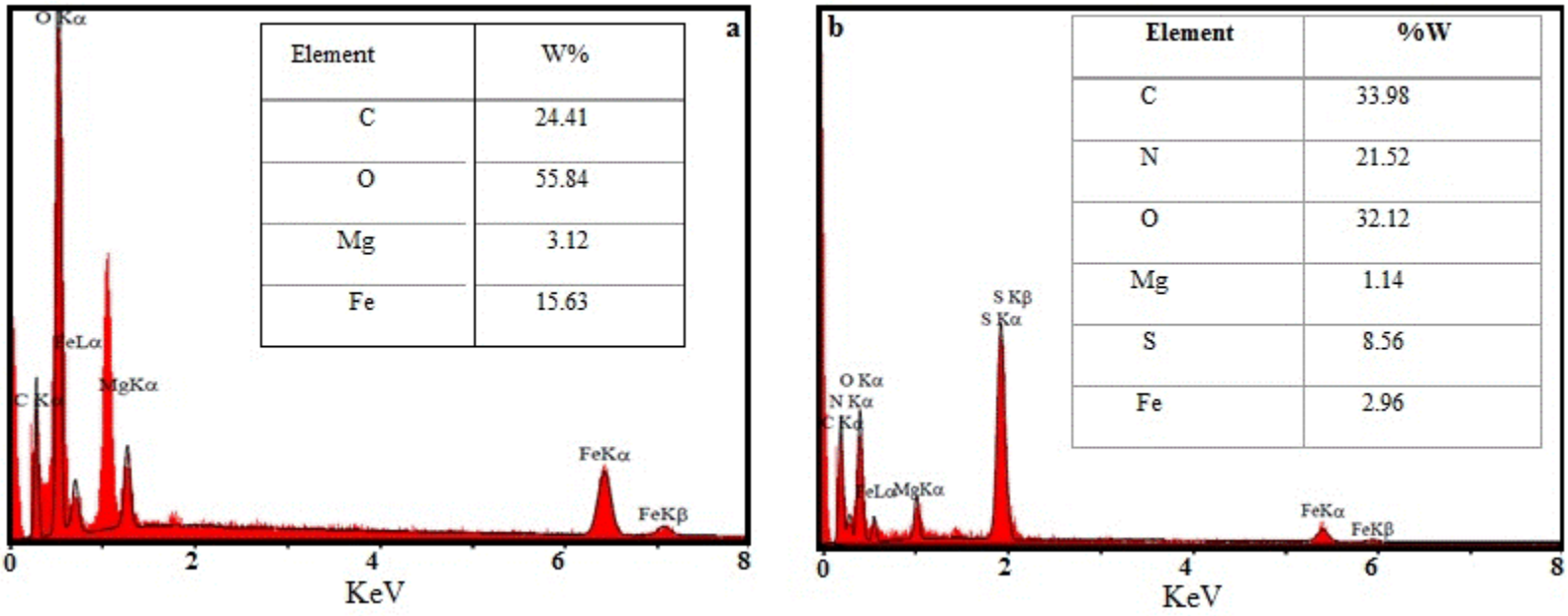

Element	W%
C	24.41
O	55.84
Mg	3.12
Fe	15.63

Element	%W
C	33.98
N	21.52
O	32.12
Mg	1.14
S	8.56
Fe	2.96

Fig.1: EDX analysis of magnetic GA (a) and cysteine immobilized magnetic GA (b).

In order to study the crystalline structure of as-synthesized $MgFe_2O_4$ - GA and thiol immobilized magnetic GA the XRD analysis was employed. According to results at the Fig.2a, the XRD pattern of magnesium ferrite – GA show typical main peaks at 2θ° = 29.64°, 35.12°, 42.48°, 52.72°, 56.2° and 61.76° that are assigned to (220), (311), (400), (422), (511), and (440) planes of a cubic spinel structure. The observed results are in good agreement with the reference number of 5247-006-98 for magnesium ferrite. The GA show a main peak at 2θ° equal to 22° which is corresponded to the (110) pseudo-orthorhombic reflections of the polysaccharide [33]. After functionalization with thiol a sharp peak around 2θ° = 22° appeared which can be assigned to new crystallinity owe to LC. In other words GA and LC structure contain several number of hydroxyl, carboxyl and amine functionality which can interact with each other through strong hydrogen bonding led to regularity of the composite structure that appear as of new ca new crystalline structure. Characteristic peaks of the magnetic GA are also observable with high intensity which confirmed formation of the target composite material.

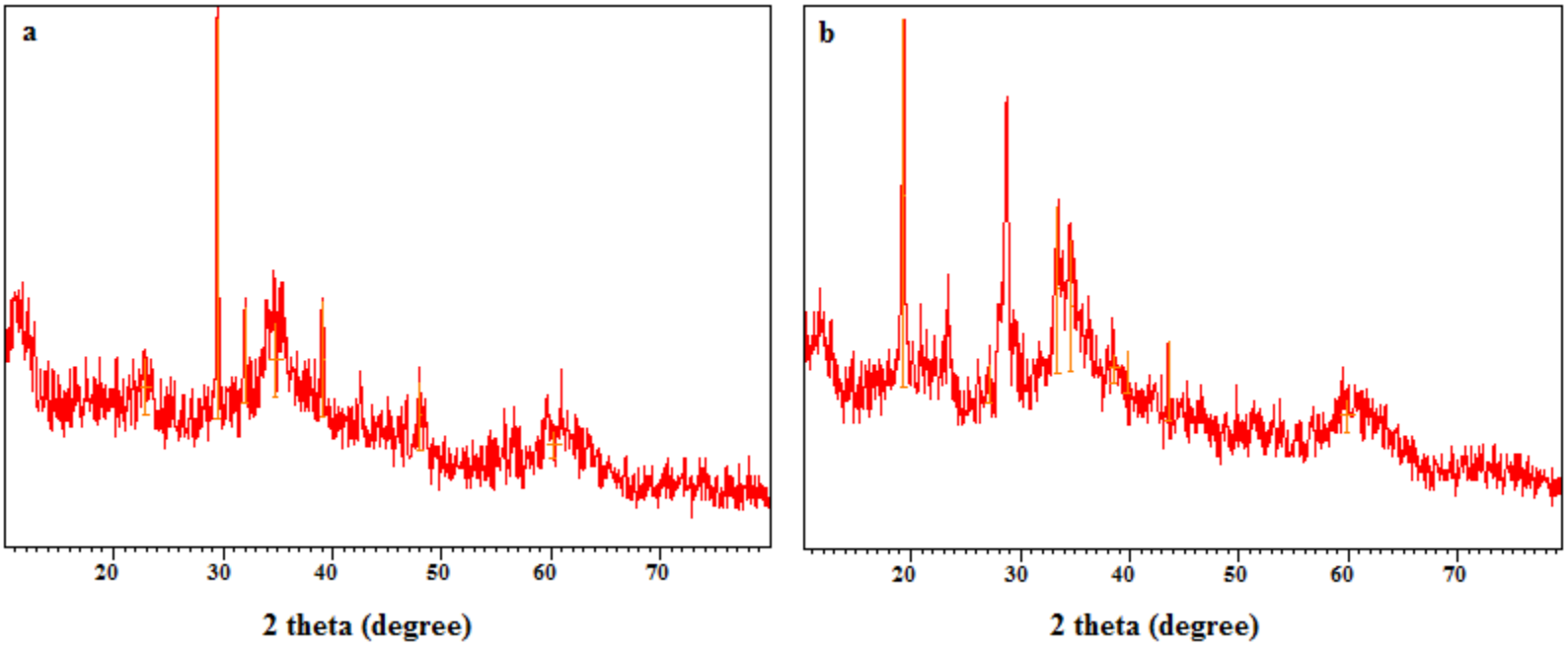

Fig.2: XRD pattern of magnetic GA (a) and cysteine immobilized magnetic GA (b).

Magnetic behavior of the thiol functionalized magnetic GA in term of magnetization versus applied field is shown at Fig.3. The value of magnetic saturation (M_s) for the final composite is 1.8 emu g^{-1} which is lower than some reports in literature [34]. This can be owe to the low contribution of the magnetic nanoparticles in total volume fraction as well as disaffiliation of the

GA as an inert coating layer on the total magnetization. It has been observed that the M_r value of the magnetic composite was 0.06 emu/g. It indicated that the prepared magnetic material probably is classified as a superparamagnetic compound since in the absence of an external magnetic field the remanence value was near to zero.

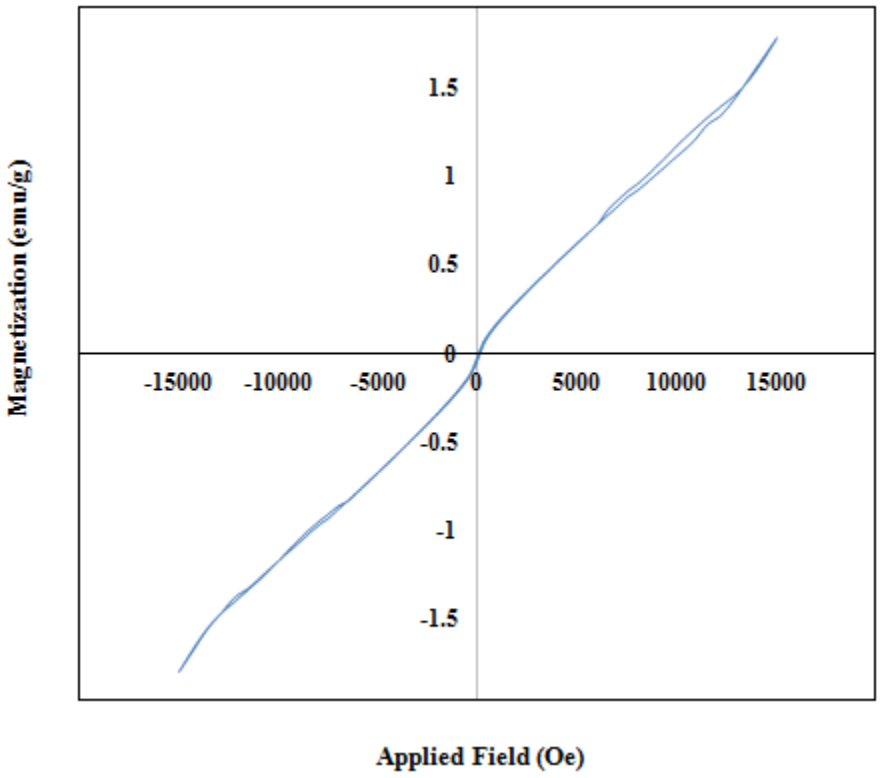

Fig.3: VSM pattern of cysteine immobilized magnetic GA.

The FESEM image of the magnetic GA and thiol immobilized composite is shown at Fig. 4. The image indicated that the both materials are in aggregated form which composed of flake like structure. The composite structure is composed of GA, LC and magnetic fragment hence the observed structure can be assigned to the intermolecular and intramolecular hydrogen bonds between them. In other words, GA which acts as a stabilizer to prevent direct magnetic interaction between the particles composed of hydroxyl functional groups. They can react with each other and with hydroxyl groups of ferrite as well as with amine and carboxyl groups of LC through hydrogen bonding in various directions thus; the nanocomposite is regarded as a combined structure.

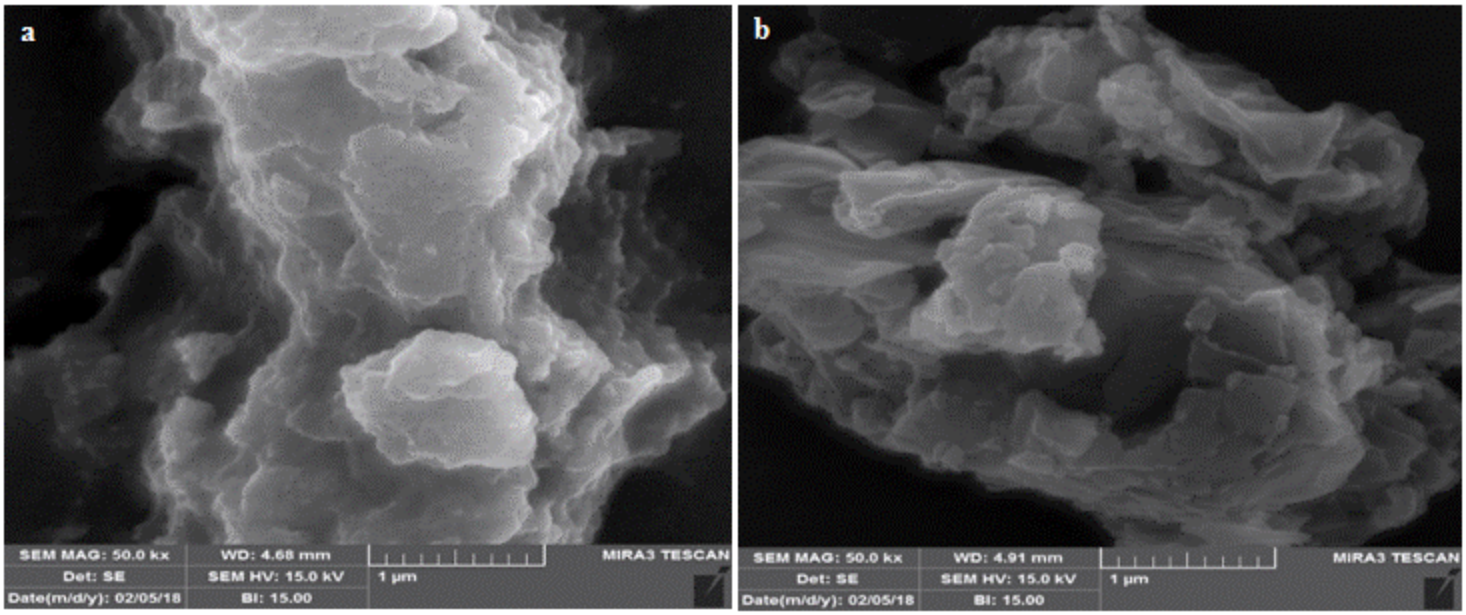

Fig.4: FESEM image of magnetic GA (a) and cysteine immobilized magnetic GA (b).

In order to study the pore size diameter and volume the N_2 adsorption-desorption experiment has been performed for magnetic GA and cysteine immobilized composite moreover, corresponding Barrett, Joyner, and Halenda (BJH) pore size distribution curve is obtained. Results are shown in Fig. 5. As can be seen the curve for magnetic GA belong to type II isotherm that possesses slit shape pores with parallel walls. The isotherm have a minor hysteresis loop owe to filling and emptying of the pores by capillary condensation [35]. Table 2 shows the BET characteristics of the materials. As can be seen, the pore diameter of the material is in the range of 11 - 18 nm and pore size increased from magnetic GA to final composite. Pore-size distribution indicated that the materials are belong to mesopores compounds [36]. Moreover, it can be seen that the total pore volume of the final composite increased respect to magnetic GA as a result of new crystalline formation on the composite structure. In other words, large number of hydroxyl and amine groups on the GA and cysteine structure linked together through stronger intra and intermolecular hydrogen bonds led to regularity of the composite structure that increases the pore volume.

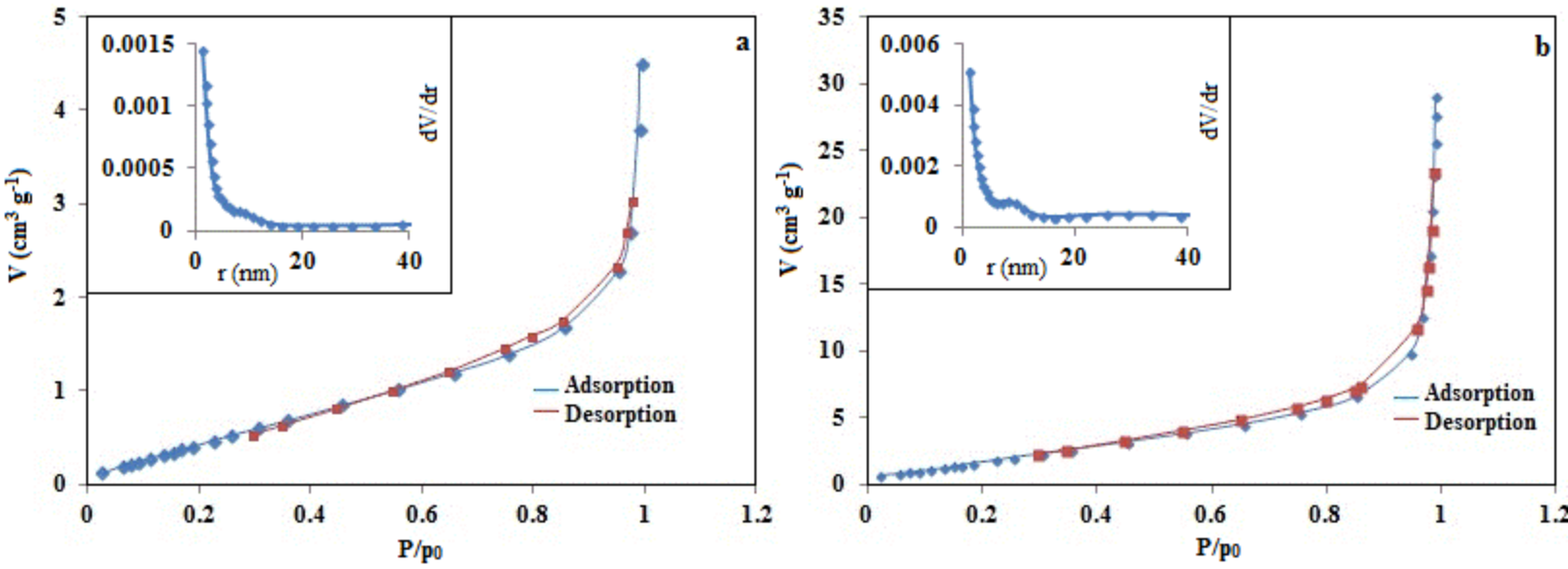

Fig.5: N_2 adsorptions - desorption and pore size distribution of magnetic GA (a) and cysteine immobilized magnetic GA (b).

Table 2: BET analysis data of magnetic GA and LC immobilized sorbent

Parameter	Magnetic GA	Magnetic GA - LC
V_m	0.54(cm^3(STP) g^{-1})	2.20 (cm^3(STP) g^{-1})
$a_{s,BET}$	2.37(m^2 g^{-1})	9.60 (m^2 g^{-1})
Total pore volume(p/p_0=0.990)	0.0067(cm^3 g^{-1})	0.04280 (cm^3 g^{-1})
Mean pore diameter	11.32(nm)	17.85(nm)

3.2. Fitting of process models

Using BBD a polynomial equation has been extracted and used for calculation of regression coefficients. Removal percentage (%R) has been linked to decoded variables and results are depicted in the equations 2 and 3 corresponding to magnetic GA and thiol functionalized composite, respectively. At the equations A, B, and C are independent variables including pH, contact time and sorbent dosage, respectively.

$$\%R = +68.05 + 15.53A - 0.08B + 17.26C - 7.81AB - 0.35AC + 1.96BC - 30.43A^2 + 1.26\ B^2 - 10.05\ C^2 - 80.70A^2B - 15.91A^2C - 11.61AB^2 \quad (2)$$

$$\%R = 41.20 - 15.42A + 4.59B + 6.33C - 0.56AB + 8.25AC + 5.14BC + 14.99A^2 - 6.08B^2 + 8.76C^2 \quad (3)$$

The significance of coefficients was verified from F and P values based on the calculation of analysis of variance (ANOVA) and results are depicted at Tables 3 and 4 that are belong to magnetic GA and final composite, respectively. Probability value (P) show low values of <0.0035 and <0.0008 which proves the regressions of mercury adsorption are statistically significant. According to the P-values for the model terms, the independent variable of A (pH) is significant for mercury removal using thiol modified magnetic GA. Besides, results showed that the variable of C and quadratic terms of A^2 significantly affects the mercury removal using both magnetic GA and thiol modified sorbent.

Table 3: the ANOVA of mercury adsorption onto magnetic GA

Source	Sum of Squares	df	Mean Square	F Value	p-value Prob > F	
Model	7272.912	12	606.076	8.50836	0.0263	significant
A-pH	964.413	1	964.413	13.53885	0.0212	
B-time	0.030625	1	0.030625	0.00043	0.9845	
C-dose	1191.976	1	1191.976	16.73348	0.0150	
AB	244.1406	1	244.1406	3.427353	0.1378	
AC	0.497025	1	0.497025	0.006977	0.9374	
BC	15.40563	1	15.40563	0.216271	0.6661	
A^2	3898.563	1	3898.563	54.72974	0.0018	
B^2	6.644901	1	6.644901	0.093284	0.7753	
C^2	425.5911	1	425.5911	5.974634	0.0709	
A^2B	151.38	1	151.38	2.125139	0.2186	
A^2C	506.2562	1	506.2562	7.107046	0.0560	
AB^2	249.3145	1	249.3145	3.499985	0.1347	
Pure Error	284.932	4	71.233			
Cor Total	7557.844	16				

Table 4: the ANOVA of mercury adsorption onto magnetic GA

Source	Sum of Squares	df	Mean Square	F Value	p-value Prob > F	
Model	4198.442	9	466.4935	15.12148	0.0008	significant
A-pH	1901.903	1	1901.903	61.65055	0.0001	
B-time	168.3613	1	168.3613	5.457462	0.0521	
C-dose	320.6778	1	320.6778	10.39483	0.0146	
AB	1.265625	1	1.265625	0.041025	0.8453	
AC	273.9025	1	273.9025	8.878602	0.0205	
BC	105.5756	1	105.5756	3.422254	0.1068	
A^2	945.7901	1	945.7901	30.65797	0.0009	
B^2	155.3921	1	155.3921	5.037065	0.0597	
C^2	323.2901	1	323.2901	10.47951	0.0143	
Residual	215.9481	7	30.84973			
Lack of Fit	64.68313	3	21.56104	0.570153	0.6638	not significant
Pure Error	151.265	4	37.81625			
Cor Total	4414.39	16				

Figs. 6a and 6b reveal good agreement between the predicted response (%R) values with the observed values over the selected range of independent variables. Most of the response points are located in a narrow range since illustrating standard deviations of 9.4 and 5.5 between the experimental and predicted results, respectively. Additionally, the values of R^2 (0.92 and 0.95) are near to the adjusted R^2 (0.82 and 0.88) and indicate a high dependence and correlation between the observed and the predicted values of responses. Adequate precisions are 9.8 and 12.12 for the magnetic GA and final composite, respectively, which demonstrate the significance of the model for the mercury adsorption process because the ratio greater than 4 is desirable[37].

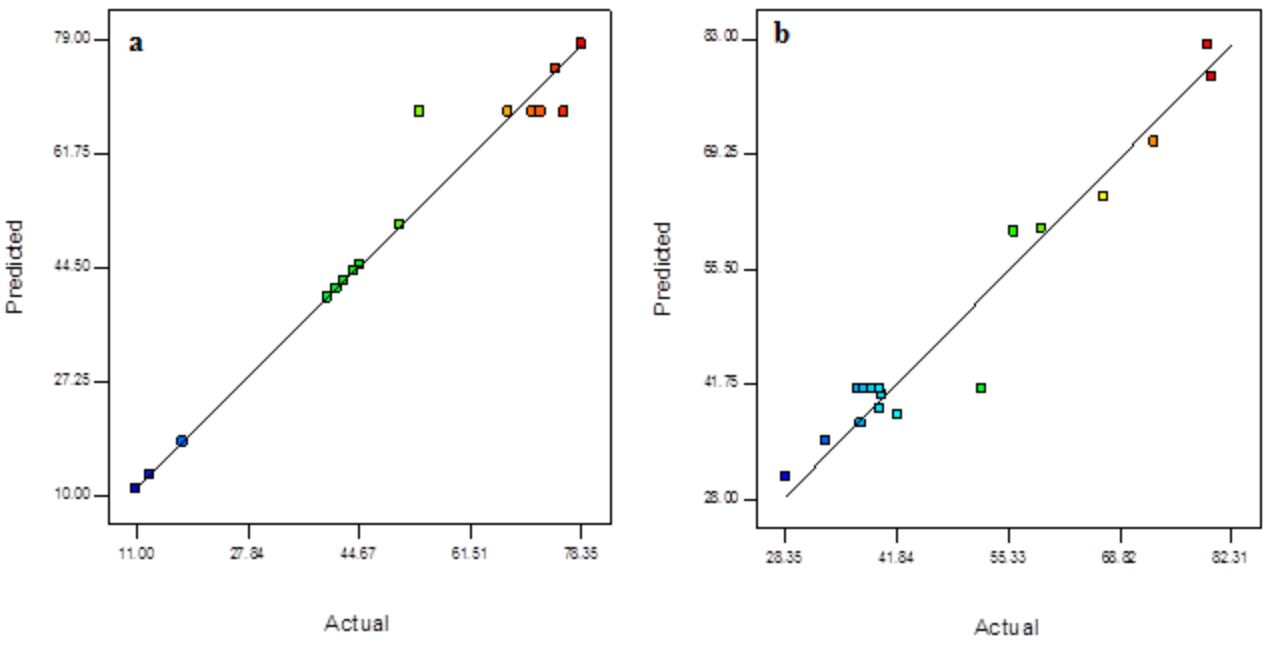

Fig. 4: The predicted response (%R) values vs. the actual values for mercury removal using magnetic GA (a) and cysteine immobilized magnetic GA (b).

Validation of ANOVA was studied with employing normal distribution of residual from the normal probability plot (NPP). According to results at Fig 5a and 5b data are stay on straight lines that possesses low violation from the assumptions as emphasizes the normality of the data. Results of perturbation plots are shown in Fig.6a and 6b. The plots imply comparative effects of the parameters on removal. It can be seen that the curve of A and C show steep curvatures which confirmed that the mercury removal percentage is sensitive to pH and adsorbent dosage.

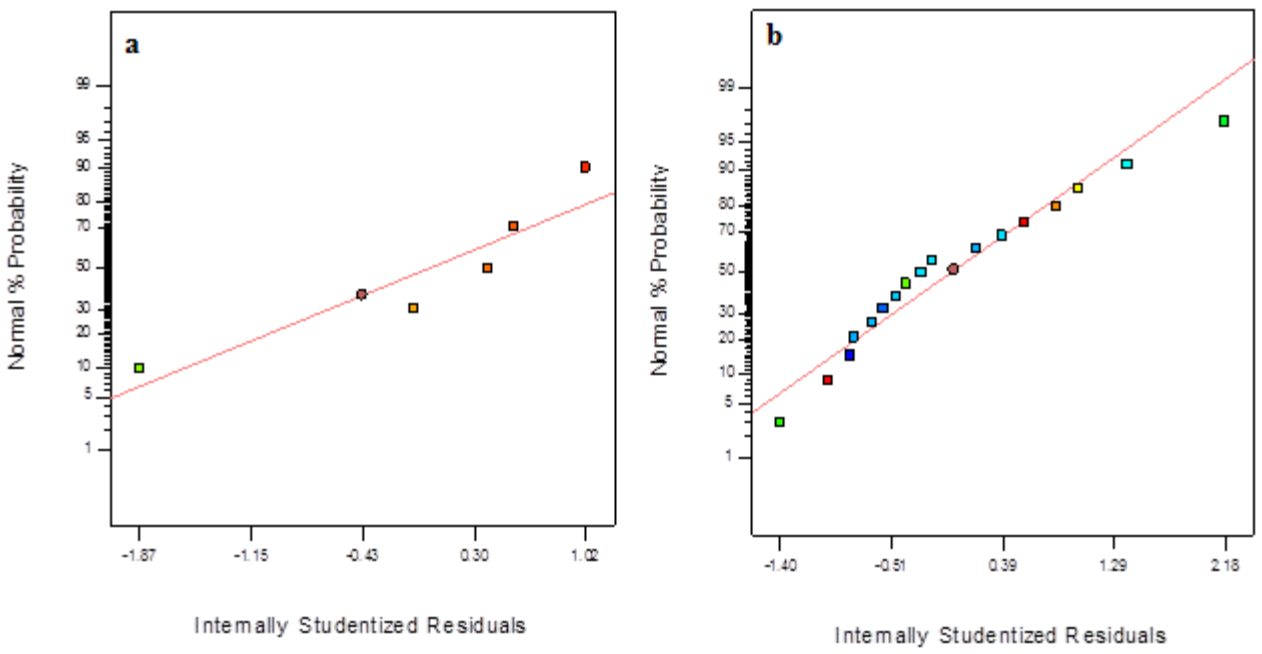

Fig. 5: The NNP for mercury removal using magnetic GA (a) and cysteine immobilized magnetic GA (b).

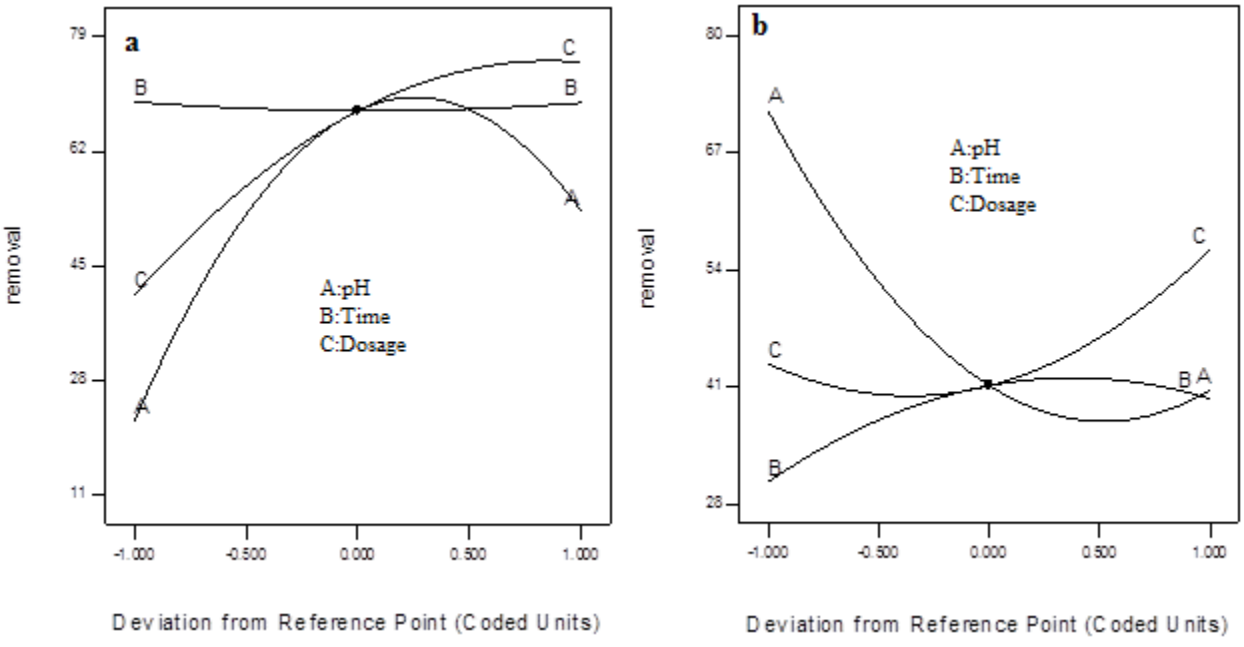

Fig. 6: The perturbation plot for mercury removal using magnetic GA (a) and cysteine immobilized magnetic GA (b).

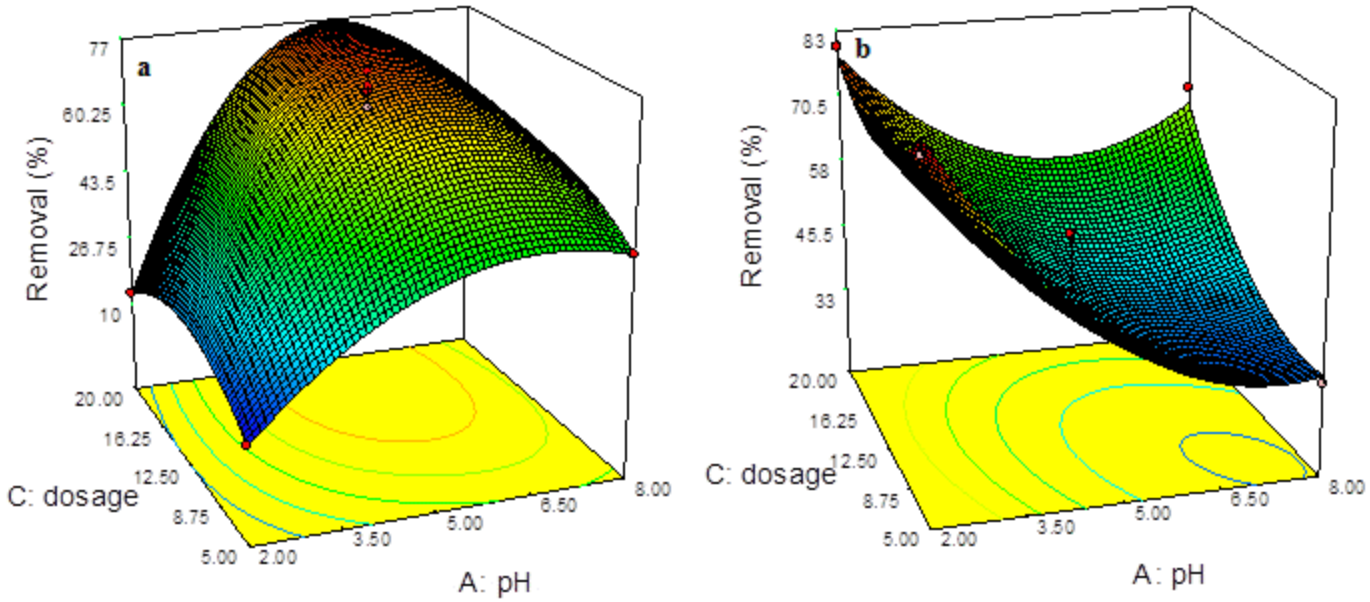

Fig.7: 3D plots of mercury adsorption with magnetic GA (a) and thiol functionalized sorbent (b).

The 3D plots based on pH and dosage is shown in Fig. 7. Results showed that the optimum levels of the variables were pH of 5, time of 15 min, and adsorbent dosage of 19 mg using magnetic GA. Thiol functionalized sorbent showed the optimum value of pH of 2, time of 15 min, and adsorbent dosage of 5 mg. The accuracy of the results was evaluated after performing three experiments at the optimum conditions using thiol functionalized sorbent. It was found that there was a good agreement between the calculated responses (83%) and mean three experimental responses (85%).

3.3. Kinetics study

Kinetic study is useful to estimation the involved adsorption mechanisms by evaluating rate expressions moreover they express sorption rates. In view of practical application large scale adsorption system can be designed based on the results of the kinetic study [38]. Kinetic parameters was extracted through performing several experiments at the optimum condition and time range below 15 min. Mercury concentration was 20 mg/L and sample volumes were 20 mL. Two main kinetic models i.e., pseudo-first-order and pseudo-second-order were used to evaluate the results. The mentioned kinetic models can be expressed as the following equations:

$$\ln Q_e - Q_t = \ln Q_e - k_1 t \quad (4)$$

$$\frac{t}{Qt} = \frac{1}{k^2 Qe^2} + \frac{t}{Qe} \quad (5)$$

At the above equations the parameters of k_1 represent the pseudo-first-order model constant (min^{-1}) and k_2 imply the pseudo - second-order rate constant (g $mg^{-1}min^{-1}$). The Q_e and Q_t express the values of the amount adsorbed per unit mass at equilibrium and at any time t, respectively.

Table 5 show the results of the studied kinetic models and confirmed that the pseudo-second-order model has better linearity respect to the pseudo - first-order model moreover, obtained Q_e based on the pseudo – second-order model show lower deviation from the experimental values; hence, this model can better describe the adsorption kinetic by magnetic GA and thiol modified sorbent.

Table 5: kinetic parameters of mercury adsorption

Model	Parameter	Magnetic GA	Magnetic GA - LC
Pseudo first-order	Q_e	1.09	1.10
	K_1	0.21	0.96
	R^2	0.87	0.72
Pseudo-second-order	Q_e	19.18	8.92
	K_2	0.31	1.42
	R^2	0.99	0.99
	Qexp	19.81	9.17

3.4. Adsorption isotherms

Two main adsorption isotherm models i.e., Langmuir and Freundlich isotherm models are employed to study adsorbate-adsorbent interaction. The models were described using the nonlinear equations with MATLAB R2013a software. Relative to the linear isotherm model in nonlinear equations the error distribution and isotherm parameters are fixed in the same axis [39] The models was illustrated with following equations. .

$$Q_e = (bQ_mC_e)/(1+bC_e) \quad (6)$$

$$Q_e = K_fC_e^{1/n} \quad (7)$$

In the above equations, C_e (mg L^{-1}) is equilibrium concentration of the analyte in the liquid phase, Q_e (mg g^{-1}) is adsorption capacity, K_f and n are coefficients of the Freundlich model and b and Q_m are Langmuir coefficients[40, 41].

Equilibrium parameter (R_L) was used to express the essential characteristics of the Langmuir equation. The parameter is a dimensionless constant which is calculated using following equation.

$$R_L=1/(1+K_LC_0) \quad (8)$$

In this equation, C_0 is the initial solute concentration. The value of R_L may be equal to zero which indicates the isotherm is irreversible. $0<R_L<1$ indicate that the model is favorable, $R_L=1$ confirm the model is linear and $R_L>1$ show the model is unfavorable [42]. Result are shown in table 6 and based on the R_L value it can be seen that mercury adsorption onto both adsorbent is favorable. R^2 and SSE (sum of squire error) values indicated that analysis the experimental data fitted with the Langmuir model using magnetic GA as adsorbent. However, mercury adsorption onto the thiol functionalized magnetic GA fitted with the Freundlich model. Based on the results maximum adsorption capacity of magnetic GA and composite is 96 and 250 mg g^{-1}. Results illustrated that mercury adsorption onto both adsorbents is not a net physical or chemical process as mercury adsorption onto the final composite can be classified as a multilayer physical adsorption on the heterogeneous surface. This type of sorption is include direct adsorption of first layer on the surface of the sorbent along with precipitation or hydrogen bonding type attachment of other layers on the surface of the first layer [43–45].

Table 6: isotherm data of mercury adsorption on the adsorbents

Model	Parameter	Magnetic GA	Magnetic GA - LC
Langmuir	Q_m	96	250
	B	0.13	0.0008
	R^2	0.85	0.71
	R_L	0.34-0.61	0.131 – 0.132
	SSE	796.8	74.40
Freundlich	n	1.31	0.919
	K_f	27.71	51.63
	R^2	0.83	0.71
	SSE	920.3	73.01

3.5. Adsorption mechanism

Metal ions - solid surface interaction takes place through physical or chemical processes. Based on the results of the kinetics studies, the mercury adsorption onto both sorbents followed pseudo-second order model hence can be classified as a chemisorption process. Isotherm study showed that adsorption onto magnetic GA followed monolayer Langmuir model. Besides, the

adsorption onto the thiol functionalized magnetic GA followed multilayer Freundlich model. Therefore it can be concluded that the mercury sorption is along with a physicochemical process. In other words, mercury adsorption followed a complex mechanism as both the chemical and physical adsorptions contribute at the same time in the adsorption process.

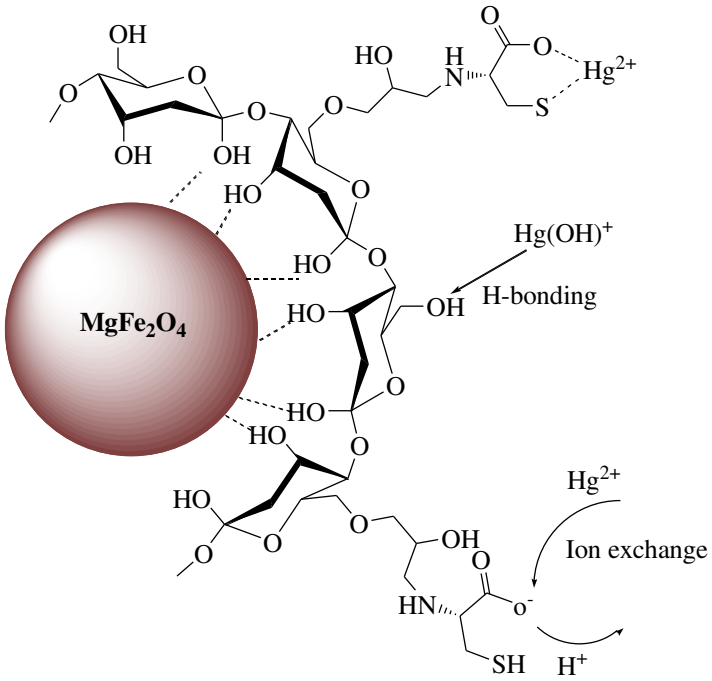

Fig.8: Schematic of mercury adsorption onto L-cysteine immobilized magnetic GA**.**

Mercury interaction with the functional groups of the sorbent can be classified as an electrostatic attraction, ion exchange and complexation reaction (Fig.8). Magnetic GA contain oxy/hydroxy groups as the electrostatic attraction occur between the mercury ion and the deprotonated oxy-hydroxy groups however ion exchange between H^+ and Hg^{2+} has main roles on the mercury adsorption at the mold acidic condition. Mercury adsorption on the surface of thiol functionalized sorbent take place at acidic solution hence ion exchange and hard – soft acid – base interaction between sulfur and mercury ions are the main mechanism at this situation.

3.6. Desorption and reusability

Regeneration of the sorbent is a main factor that makes the sorption process more economical hence, different concentrations of HCl–thiourea solution with a concentration of 0.5 mol L^{-1} for HCl and 0.5, 1 and 2% thiourea are tested for release of the adsorbed mercury ions. Selection of thiourea was based on hard–soft acid-base theory since the sulfur group of it can easily react with

the mercury ions. It is found that a mixture of HCl (0.5 mol L^{-1}) and 2% thiourea releases adsorbed mercury ions with efficiency of 95–97%. Moreover, the reusability of the final sorbent was examined with the several sorption – desorption run and it is found that after 3 cycles the removal efficiencies reached from 97 and 95% to 90% which confirm its efficiency as regenerable adsorbent.

3.7. Comparison of the adsorbents performances

In this research, two adsorbents including magnetic GA and thiol immobilized adsorbent were used for the mercury removal from aqueous solution. According to results, the final composite showed better performance relative to magnetic GA. The maximum adsorption capacities are 96 and 250 mg g^{-1} for the magnetic GA and final composite, respectively. The reason may be related to the fact that mercury is a soft acid species and as a result, they have lower tendencies toward oxy/hydroxy functional groups. Nevertheless, the final composite is composed of sulfur groups which are ready to capture mercury ions through self-assembly routes.

The mercury adsorption efficiency of the presented sorbents has been compared with some reports in the literature in Table 7. It is obvious that the performances of the prepared sorbents are appropriate with respect to adsorption time as followed fast adsorption kinetic. Moreover, they demonstrate satisfactory sorption capacities which are higher than the values for most reported adsorbents. Besides, the employed sorbent is a green adsorbent as its components include environmentally friendly material which doesn't generate secondary byproduct.

Table 7: Comparing mercury adsorption performance of the sorbent with literature

Adsorbent	Q_m ($mg.g^{-1}$)	Time (min)	References
Malt spent rootlets	50	10h	[2]
Aluminosilicate sieve	20.65	100	[5]
Ion-imprinted bead	0.45	15	[6]
Eucalyptus bark	33.11	60	[12]
Resin - sulfamine	222.2	90	[14]
L-cysteine- silica	429	5	[44]

Thiourea- Magnetic Biosorbent	290	12h	[45]
$MgFe_2O_4$ – GA	96	15	This work
$MgFe_2O_4$ – GA - LC	250	15	This work

4. Conclusions

In summary, a nanocomposite of ferrite - Gum Arabic and L- cysteine immobilized composite was synthesized and employed for mercury removal from water solution. Effects of important parameters on removal efficiency were studied with RSM and results showed that solution pH and adsorbent dosage are effective parameters on the sorption efficiency. Adsorption onto the sorbents followed pseudo-second-order kinetics model. Isotherm study showed that the adsorption onto magnetic GA followed the Langmuir model however the adsorption onto final composite was fitted with the Freundlich model. Results confirmed that mercury adsorption followed physicochemical sorption mechanism. The magnetic GA –cysteine nanocomposite could be considered as a green adsorbent with a good adsorption capacity of 250 mg g^{-1} which proved the efficiency of sorbent for decontamination of water in terms of mercury ions.

Acknowledgments

The financial support of this work by the Research Council of the University of Tehran and Shahid Chamran University of Ahvaz through grant is gratefully acknowledged.

References

1. Kaveh R, Bagherzadeh M, Simultaneous removal of mercury ions and cationic and anionic dyes from aqueous solution using epichlorohydrin cross-linked chitosan @ magnetic Fe_3O_4/activated carbon nanocomposite as an adsorbent, *Diam. Relat. Mater* 124: 108923 (2022).
2. Bekhoukh A., Moulefera I., Zeggai F.Z. et al, Anionic Methyl Orange Removal from Aqueous Solutions by Activated Carbon Reinforced Conducting Polyaniline as Adsorbent: Synthesis, Characterization, Adsorption Behavior, Regeneration and Kinetics Study. *J Polym Environ.* 2022, 30, 886.
3. Abukhadra M.R., Mostafa M., Jumah M.N.B. et al, Insight into the Adsorption Properties of Chitosan/Zeolite-A Hybrid Structure for Effective Decontamination of Toxic Cd (II) and As (V) Ions from the Aqueous Environments. *J Polym Environ.* 2022, 30, 295.
4. Li Z, Wu L, Liu H, et al, Improvement of aqueous mercury adsorption on activated coke by thiol-functionalization. *Chem. Eng. J.* 228:925-934 (2013).

5. Khorshidi P, Shirazi R.H.S.M., Miralinaghi M. et al. Adsorptive removal of mercury (II), copper (II), and lead (II) ions from aqueous solutions using glutathione-functionalized $NiFe_2O_4$/graphene oxide composite. *Res Chem Intermed* 46: 3607–3627 (2020).

6. Andaç M, Mirel S, Şenel S, Say R, Ersöz A, Denizli A, Ion-imprinted beads for molecular recognition based mercury removal from human serum, *Int. J. Biol* 40:159–166 (2007).
7. Zhang X, Wang Q, Zhang S, et al, Stabilization/solidification(S/S) of mercury-contaminated hazardous wastes using thiol-functionalized zeolite and Portland cement. *J Hazard Mater* 168:1575–1580 (2009).
8. Tang C, Qin Y, Ni C, Zou J, Detection and Removal of Mercury Ions in Water by a Covalent Organic Framework Rich in Sulfur and Nitrogen, *ACS Appl. Polym. Mater.*4: 849–858 (2022).
9. Movahedi F, Masrouri H, Tayyebi H, Highly efficient adsorption behavior of benzoylthiourea functionalized graphene oxide with respect to the removal of Hg(II) from aqueous solutions: isothermal, kinetic and thermodynamic studies. *Res Chem Intermed* 44: 5419–5438 (2018).

10. Hajri AK, Jamoussi B, Albalawi A.E, Alhawiti O, Alsharifa A, Designing of modified ion-imprinted chitosan particles for selective removal of mercury (II) ions, *Carbohydr. Polym* 286: 119207(2022).
11. Toubi Y, Radi S. Bacquet M, Synthesis of pyridin-3-yl-functionalized silica as a chelating sorbent for solid-phase adsorption of Hg(II), Pb(II), Zn(II), and Cd(II) from water. *Res Chem Intermed* 39: 3791–3802 (2013).
12. Ghodbane I, Hamdaoui O, Removal of mercury (II) from aqueous media using eucalyptus bark : Kinetic and equilibrium studies. *J Hazard Mater* 160:301–309 (2008).
13. Bulin C, Li B, Zhang Y. et al, Removal performance and mechanism of Fe_3O_4/graphene oxide as an efficient and recyclable adsorbent toward aqueous Hg(II). *Res Chem Intermed* 46: 4509–4527 (2020).
14. Qi Y, Jin X, Yu C, et al, A novel chelating resin containing high levels of sulfamine group : Preparation and its adsorption characteristics towards p -toluenesulfonic acid and Hg (II). *Chem. Eng. J.* 233:315–322 (2013).
15. Mirzai M., Asadabadi S. Magnetic Nanocomposites Containing Low and Medium-Molecular Weight Chitosan for Dye Adsorption: Hydrophilic Property Versus Functional Groups. *J Polym Environ*, 2022, 30, 1560.
16. Fuzil N.S., Othman N.H., Jamal N.A.S.R.A. et al, Bisphenol A Adsorption from Aqueous Solution Using Graphene Oxide-Alginate Beads. *J Polym Environ.* 2022, 30, 597.
17. Benhammou A, Yaacoubi A, Nibou L, Tanouti B, Study of the removal of mercury (II) and chromium (VI) from aqueous solutions by Moroccan stevensite. *J Hazard Mater* 117:243–249 (2005).
18. Al-Musawi T.J., Mengelizadeh N., Al Rawi O. et al, Capacity and Modeling of Acid Blue 113 Dye Adsorption onto Chitosan Magnetized by Fe_2O_3 Nanoparticles. *J Polym Environ*. 2022, 30, 344.
19. Hossein M, Hadi M, Jamali A, A novel polylysine – resorcinol base g -alumina nanotube hybrid material for effective adsorption/preconcentration of cadmium from various matrices. *J. Ind. Eng. Chem* 46:165–174 (2017).
20. Hossein M, Shemirani F, Malakootikhah J, Minaeian S, Catalytic synthesis of graphene-like polyaniline derivative - MFe_2O_4 (M ; Cu , Mn) nanohybrid as multifunctionality water decontaminant. *React Funct Polym* 125:108–117 (2018).
21. Zhai Y, Chang X, Cui Y, et al, Original Paper Selective Determination of Trace Mercury (II)

after Preconcentration SiO_2 Particles from Sample Solutions. *Microchim Acta* 259:253–259 (2006).
22. Wang Y., Wu Y., Cong H. et al, Preparation of Pyridine Polyionic Liquid Porous Microspheres and Their Application in Organic Dye Adsorption. *J Polym Environ*. 2022, 30, 385.
23. Khatoon N, Khan AH, Pathak V, et al, Removal of hexavalent chromium from synthetic waste water using synthetic Nano Zero Valent Iron (NZVI) as adsorbent. *International Int. j. innov. res. technol* 2:6140–6149 (2013).
24. Weber CT, Foletto EL, Meili L, Removal of tannery dye from aqueous solution using papaya seed as an efficient natural biosorbent. *Water Air Soil Pollut.* 224: 1427 (2013).
25. Zhao F, Repo E, Yin D, et al, EDTA-Cross-Linked β-Cyclodextrin: An Environmentally Friendly Bifunctional Adsorbent for Simultaneous Adsorption of Metals and Cationic Dyes. *Environ. Sci. Technol* 49:10570–10580 (2015).
26. Merakchi A, Bettayeb S, Drouiche N, Adour L, Cross - linking and modification of sodium alginate biopolymer for dye removal in aqueous solution. *Polym. Bull*. 76: 3535–3554 (2019).
27. Alzahrani E, Gum Arabic-Coated Magnetic Nanoparticles For Methylene Blue Removal. *Int.* j. *innov. res. sci. technol* 3:15118–15129(2014).
28. Sehaqui H, Mautner A, Perez De Larraya U, et al, Cationic cellulose nanofibers from waste pulp residues and their nitrate, fluoride, sulphate and phosphate adsorption properties. *Carbohydr. Polym* 135:334–340 (2016).
29. Singh V, Singh SK, Synthesis and characterization of gum acacia inspired silica hybrid xerogels for mercury (II) adsorption. *Int. J. Biol. Macromol* 48:445–451 (2011).
30. Pirouz MJ, Beyki MH, Shemirani F, Anhydride functionalised calcium ferrite nanoparticles: A new selective magnetic material for enrichment of lead ions from water and food samples. *Food Chem.* 170:131–137 (2015).
31. Beyki MH, Bayat M, Miri S, et al, Synthesis, characterization, and silver adsorption property of magnetic cellulose xanthate from acidic solution: Prepared by one step and biogenic approach. *Ind. Eng. Chem. Res* 53:14904–14912 (2014).
32. Vanitha M, Balasubramanian N, Joni IM, Detection of mercury ions using L-cysteine modified electrodes by anodic stripping voltammetric method Detection of Mercury Ions using L-Cysteine Modified Electrodes by Anodic Stripping Voltammetric Method. *AIP Conference Proceedings* 1927: 30001 (2018).
33. Ghanbarian M, Nabizadeh R, Nasseri S, et al, Potential of amino-riched nano-structured $MnFe_2O_4$@cellulose to biosorption of toxic Cr (VI): Modeling, kinetic, equilibrium and comparing studies. *Int. J. Biol. Macromol* 104:465-480 (2017).
34. Rezaei AA, Hossein Beyki M, Shemirani F, Fast sono assisted ferrofluid mediated silver super – Adsorption over magnesium ferrite-copper sulfide chalcogenide with the aid of multivariate optimization. *Ultrason Sonochem* 37:509-517 (2017).
35. Bayat M, Beyki MH, Shemirani F, One-step and biogenic synthesis of magnetic Fe_3O_4-Fir sawdust composite: Application for selective preconcentration and determination of gold ions. *J. Ind. Eng. Chem* 21:912–919 (2015).
36. Dabrowski A, Adsorption, from theory to practice. *Adv. Colloid Interface Sci* 93:135–224 (2001).
37. Khani R, Sobhani S, Beyki MH, Miri S, Application of magnetic ionomer for development of very fast and highly efficient uptake of triazo dye Direct Blue 71 form different water samples. *Ecotoxicol. Environ. Saf* 150:54–61 (2018).
38. Robati D, Mirza B, Rajabi M, et al, Removal of hazardous dyes-BR 12 and methyl orange

using graphene oxide as an adsorbent from aqueous phase. *Chem. Eng. J.* 284:687–697 (2016).
39. Hossein Beyki M, Mohammadirad M, Shemirani F, Saboury AA, Magnetic cellulose ionomer/layered double hydroxide: An efficient anion exchange platform with enhanced diclofenac adsorption property. *Carbohydr. Polym.* 157:438–446 (2017).
40. Shirkhodaie M, Hossein Beyki M, Shemirani F, Biogenic synthesis of magnetic perlite@iron oxide composite: application as a green support for dye removal. *Desalination Water Treat* 57:11859–11871(2016).
41. An F-Q, Wu R-Y, Li M, et al, Adsorption of heavy metal ions by iminodiacetic acid functionalized D301 resin: Kinetics, isotherms and thermodynamics. *React Funct Polym* 118:42–50 (2017).
42. Lin S, Heavy metal removal from water by sorption using surfactant-modified montmorillonite. *J. Hazard. Mater* 92:315–326 (2002).
43. Kumar KV, Linear and non-linear regression analysis for the sorption kinetics of methylene blue onto activated carbon. *J. Hazard. Mater* 137:1538–1544 (2006).
44. Li Q, Wang Z, Fang D, et al, Preparation, Characterization, and Highly Effective Mercury Adsorption of L-Cysteine-Functionalized Mesoporous Silica. *New J Chem* 123:248–254 (2014).
45. Zhou J, Liu Y, Zhou X, et al, Removal of mercury ions from aqueous solution by thiourea-functionalized Magnetic Biosorbent : Preparation and mechanism study. *J. Colloid Interface Sci* 507:107-118 (2017).